RSC Applied Polymers

PAPER

View Article Online
View Journal

Cite this: DOI: 10.1039/d6lp00079g

Self-healable acrylic/polyolefin-reinforced composites for H_2 fuel applications

Samruddhi Gaikwad,[a] Jacob Fischer,[a] Qianhui Liu,[a] Siyang Wang,†[a] Dale Hitchcock,[b] Jake Amoroso,[b] Charles James[b] and Marek W. Urban *[a]

Received 6th March 2026,
Accepted 3rd April 2026

DOI: 10.1039/d6lp00079g

rsc.li/rscapplpolym

Fiber-reinforced composites, despite their high strength-to-weight ratios, are still susceptible to damage. Integrating self-healing matrices into these multi-phase materials offers a promising approach to extend their service life and functionality while preserving mechanical performance across multiple damage-repair cycles. In this study, we developed cost-effective composites using a van der Waals (vdW) driven self-healing thermoplastic poly(methyl methacrylate/*n*-butyl acrylate) [p(MMA/*n*BA)] matrix reinforced with high-strength polypropylene (PP) fibers. These materials can be utilized as the self-healing inner layers in engineered multilayered H_2 fuel dispensing hoses. These studies show that a p(MMA/*n*BA) copolymer matrix with a 50/50 monomer molar ratio reinforced with PP fibers wound at a 45° angle with respect to the object's longitudinal axes maintains its mechanical integrity after 25 000 damage-repair cycles. Combining experimental data with finite element analysis (FEA), these studies show that these materials exhibit favorable stress distributions under bending loads over multiple cycles. The maximum stresses occur near the fixed end in the outermost layer, while the innermost layer experiences the lowest stresses. The self-healing is effective over a wide temperature range from –196 °C to +85 °C, making them suitable components for demanding, complex energy applications in H_2 fuel storage and larger delivery systems.

Introduction

Due to exceptional strength-to-weight ratios, fiber-reinforced composites are high-performance materials widely used across various industries. Nevertheless, they remain susceptible to damage, which typically occurs through two primary mechanisms: mechanical failure due to external loads or fatigue-induced degradation. In most cases, the polymer matrix and/or the fiber–matrix interface represents the weakest link in the composite structure and is often prone to irreversible damage. To enhance the longevity and functionality, incorporating a self-healing matrix in composites has emerged as a promising strategy. While the concept of self-healing composites is appealing, not all polymers are suitable for this purpose. In addition to the durability and retention of mechanical performance over time provided by the polymer matrix, adequate fiber–matrix interfacial adhesion is critical. Several excellent review articles[1–3] and books[4] have elaborated on this topic.

With these considerations in mind, the development of polymer matrices, both thermoset and thermoplastic, or more recently, covalently adaptive networks (CANs), offers new possibilities for enhancing the durability and broadening the application scope of fiber-reinforced composites. Of particular interest are matrices that function in challenging chemical or physical environments, which, upon mechanical or electrical stress,[5] typically initiated by the formation of microvoids, are capable of self-healing. Although the most commonly used polymer matrices in composite fabrication are thermosets, including but not limited to epoxies,[6] phenolics,[7] polyurethanes,[8] and polyesters,[9] modifications are required to achieve self-healing.[10]

Due to their excellent resistance to puncture and crack propagation, epoxy resins are particularly prevalent in the aerospace, ballistic, and automotive industries. Their strong adhesion to a wide range of fiber reinforcements, including glass, carbon, and natural fibers, is desirable. Polyester matrices, another widely used class of thermosets, are often reinforced with natural fibers that offer high stiffness, enabling the production of low-cost, high-strength composites. For instance, reinforcing polyesters with natural cellulose fibers significantly enhances both impact resistance and flexural strength,[11] and to further enhance the tensile and flexural properties, these matrices are often reinforced with basalt and

[a]Department of Materials Science and Engineering, Clemson University, Clemson, SC 29634, USA. E-mail: mareku@clemson.edu
[b]Savannah River National Laboratory, Aiken, SC 29803, USA
†Current address: University of Chicago, Pritzker School of Molecular Engineering.

glass fibers.[12] Although the concept of self-healable hollow fibers containing reactive components has been proposed, their practicality may be limited.

Phenolic resins provide thermal stability up to approximately 400 °C and are often combined with carbon fibers to produce composites with exceptional mechanical strength for high-temperature stability.[13,14] Although polyurethanes are not traditionally used as composite matrices, recent innovations involve UV-induced self-healing polyurethanes,[10,15] as well as acid-modified cross-linked polyurethane networks.[16,17] The latter have demonstrated the ability to form high-strength composites with durable fiber–matrix interfaces. While continuous fibers are commonly employed in composite development, the integration of carbon nanotubes into polyurethane matrices has been shown to significantly improve both modulus and tensile strength.[18]

Commonly utilized fiber-reinforced thermoplastic matrices are polyamides,[19] polyethylene,[20] and polyether ether ketones (PEEK).[21] Among these polyether ketones, those with a semi-crystalline nature are notable for their high thermal resistance.[22] When reinforced with carbon fibers,[23] PEEK composites exhibit outstanding mechanical properties[24] and biocompatibility, making them suitable for biological applications,[25] particularly in 3D printing.[26]

Although high-density polyethylene matrices reinforced with ultra-high molecular weight polyethylene (UHMWPE) exhibit excellent mechanical performance partly due to the strong interfacial bonding, many thermoplastics lack reactive groups necessary for desirable interfacial bonding to enhance fiber-matrix adhesion.[27] Thus, thermoset matrices remain the most commonly used despite their limited processability. To overcome these drawbacks, a new class of thermosets known as covalent adaptive networks (CANs) has been developed, which features dynamic covalent bonds that enable recyclability.[28–33] Recent studies demonstrated that recyclable epoxy-based CAN matrices can be utilized in carbon fiber composites, where transesterification reactions facilitate their reprocessibility.[34] Although the potential of CANs in composites has not been fully exploited, they offer a promising opportunity to combine the benefits of thermoset and thermoplastic materials.

Although thermoplastic styrene[35,36] and acrylic-based[37–39] copolymers, especially those with preferentially alternating/random copolymer topologies, exhibit self-healing properties, their potential use in composites as matrices is unexploited. These commodity copolymers have been utilized in various other applications; this however, when incorporated into a larger, multilayered composite system, they can serve practical functions in challenging environments. One promising option is as the inner layer of H_2 fuel dispense hoses.[40] The overall durability of these composite hoses is often limited by inner-layer cracking, which is the most common mode of failure. Thus, embedding a self-healing capability may significantly extend the overall service life of the usually costly fuel dispensing hoses. In this study, we developed and fabricated self-healable inner-layer composites comprising self-healing acrylic-based matrices and high-strength polypropylene (PP) fibers. The ultimate goal is to create a p(MMA/*n*BA)-PP reinforced inner-layer composite that retains mechanical integrity and undergoes renewable self-healing after 25 000 cycles. This target surpasses the typical lifespan of ~10 000 cycles for a commercial fuel dispenser hose.[41,42] This work pioneers the integration of commodity self-healable polymer into a complex, multilayered system specifically engineered for challenging environments.

Results and discussion

While SI provide synthetic details of p(MMA/*n*BA) copolymers, the first step in this study was to assess whether p(MMA/*n*BA) copolymer films with a monomer molar ratio of ~50/50 can recover after 25 000 damage-repair cycles (or cuts). Fig. 1A depicts the repeating unit of this copolymer and the incorporation of PP fibers. To visually assess the ability to self-heal, optical images collected after ~1000 Fig. 1(B) and 10 000 Fig. 1 (C) damage-repair cycles show effective recovery. Extending these experiments to 25 000 cycles Fig. 1(1D1 and 1D2) further confirms the visual recovery from mechanical damage. To support the visual assessments, stress–strain analysis demonstrated that mechanical properties are recovered. Fig. 1E illustrates the recovery of elastic modulus (E) and maximum strain (ε_{max}) after 25 000 damage-repair cycles and, as summarized in Fig. 1F, the E and ε_{max} values after 25 000 damage-repair cycles recover ≥184 and 85% of their original values, respectively. Typically, the E and ε_{max} % ≥ 85% recovery is considered self-healable.[43,44] To confirm that the chemical integrity is maintained, ^{1}H NMR measurements were conducted before and after 25 000 cycles (SI) showing no detectable chemical changes.

These copolymers were used to fabricate p(MMA/*n*BA)-PP composites through a winding process (SI; Fig. S1, S2; Tables S1, S2). To optimize the fabrication parameters, tensile tests were conducted on composites fabricated with varying winding angles. As shown in Fig. 2A, for comparison, curve a shows the stress–strain analysis (using a 100 kN load cell) of control copolymer films (curve a), an inner layer composite produced at the fiber winding angles of 45° (curve b), 60° (curve c) and 75° (curve d), which exhibit enhanced moduli. Notably, p(MMA/*n*BA) films have lower intrinsic strength (~2 MPa) than fiber-reinforced composites (~12 MPa). The cross-sectional area (A) for polymer films was ~0.3 mm^2, whereas it was ~20 mm^2 for composite films. A high load (100 kN) combined with the inefficiency of the polymer film cross-section to distribute it, quickly exceeds the polymer film's yield and ultimate strength leading to premature fracture at lower elongation. Moreover, the composite with a winding angle of 90° (curve e) has a modulus lower than that of the copolymer film (curve a), which is likely attributed to inter-layer delamination. Among these composites, the prototype inner tubing fabricated at a 45° winding angle demonstrated the best balance of mechanical properties and was selected for further analysis.

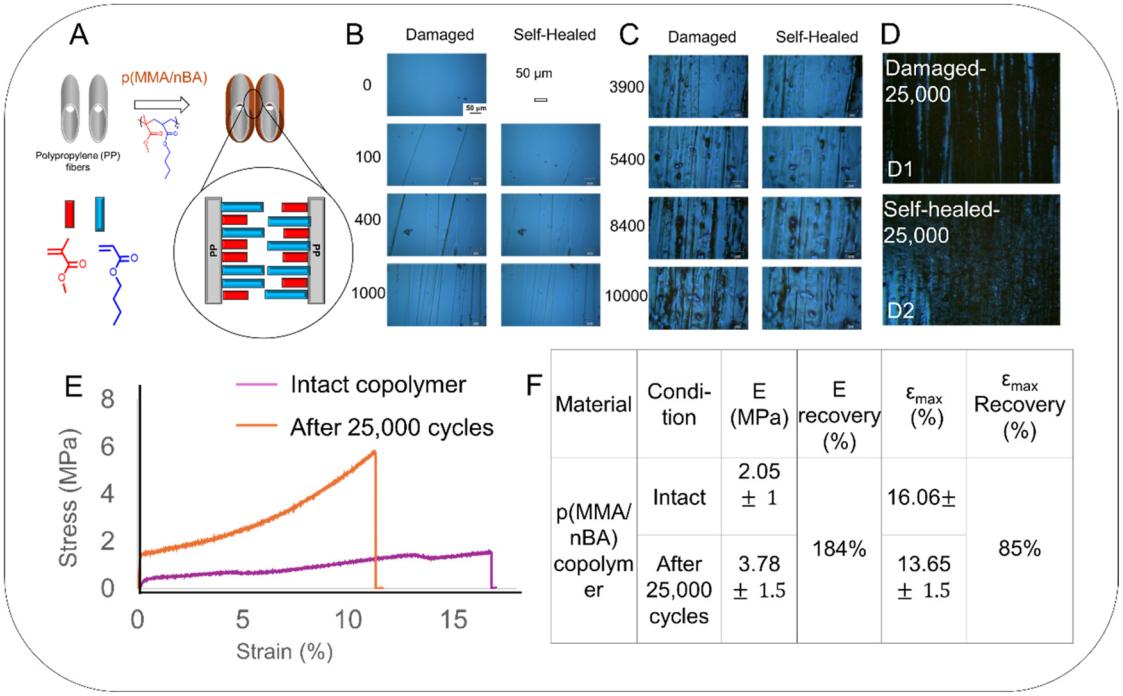

Material	Condition	E (MPa)	E recovery (%)	ε_{max} (%)	ε_{max} Recovery (%)
p(MMA/nBA) copolymer	Intact	2.05 ± 1	184%	16.06±	85%
	After 25,000 cycles	3.78 ± 1.5		13.65 ± 1.5	

Fig. 1 Polypropylene (PP) fibers embedded in p(MMA/*n*BA) copolymer matrix to form a composite interface consisting of p(MMA/*n*BA)-PP (A). Optical images of damaged and self-healed after 1000 (B), 10 000 (C), and 25 000 (D1 and D2) damage-repair cycles. Stress–strain analysis performed using a 1 kN load cell for intact (purple) and after 25 000 damage-repair cycles (orange) p(MMA/*n*BA) copolymers (E). A summary of mechanical properties for p(MMA/*n*BA) before and after 25 000 damage-repair cycles (F).

These results agree with previous assessments that, at these angles, the interlaminar shear strength arising from applied shear and strain in overlapping layers is evenly distributed, thus avoiding early failures in tensile modes.[45]

To mimic the damage-repair cycles of an inner layer composite as closely as possible to actual usage conditions, we applied bending motion using a robotic arm (SI, Fig. S4). This setup enables repeated damage-repair cycles on both self-healable and non-self-healable inner-layer composites. As shown in Fig. 2B and C, after 25 000 damage-repair cycles, the self-healing inner layer composite recovers ~117% of its E and 71% of ε_{max} values (Fig. 2C). This enhancement directs towards the enhanced fiber wetting and stronger inter-layer adhesion during damage-repair cycles. Although fiber-matrix adhesion is beyond the scope of this study, relaxation processes of macromolecular segments near the interfacial regions resulting from external physical perturbations (temperature, pressure) remains to be determined. The stress–strain analysis results confirm that the mechanical integrity is maintained, and ^{1}H NMR analysis (SI, Fig. S5) identified no chemical changes or degradation before and after 25 000 cycles. In contrast, composites with a non-self-healing copolymer matrix exhibit only 65% and 60% recovery of the initial E and ε_{max}, respectively, indicating that their mechanical properties cannot fully return to their original values (SI, Fig. S6 and Table S4).

Since bending is expected during actual use, assessing the stress distribution in self-healing and non-self-healing p(MMA/*n*BA)-PP composites was conducted. To simulate how these inner-layer composites respond to bending, finite element analysis (FEA) simulations[46] were conducted using a three-layer composite with both self-healing and non-self-healing matrices. A 30 N bending force was applied to the free end, while the opposite end was fixed (SI). Although actual tubular shape will undergo spatially complex stresses and temperature gradients, the purpose of the model approach utilized in this study was to formulate a baseline how localized stresses are generated upon damage. As shown in Fig. 2D, the stress distribution (red = high, blue = low) reveals that for self-healing composites, the maximum stresses occur near the fixed end, reaching ~35 × 10^7 N m^{-2} (point stress; 20 × 10^7 N m^{-2} through the wider region) in the outermost layer. In contrast, the innermost layer experiences the lowest stress at ~0.5 × 10^7 N m^{-2} (Table S6). All layers in the self-healing compositions show reduced stress at the bent (right) end of the structure, as illustrated in Fig. 2D. The H_2 fuel inner layer undergoes a severe temperature cycle from −196 °C to 85 °C. Although at lower temperatures segmental mobility prohibits self-repair, elevated temperatures accelerate it.

The parallel analysis of non-self-healing matrices, shown in Fig. 2E, revealed that the middle layers also experience the higher stress, reaching up to a wider region of 1.8 × 10^7 N m^{-2} stress (compared to 0.9 × 10^7 N m^{-2} for the middle layer for self-healing composite). In contrast, the inner layers had lower stress values of ~0.5 × 10^7 N m^{-2} for both the composites. These elevated stress values in the middle layers are attributed to the non-self-healing matrix, which resists deformation at

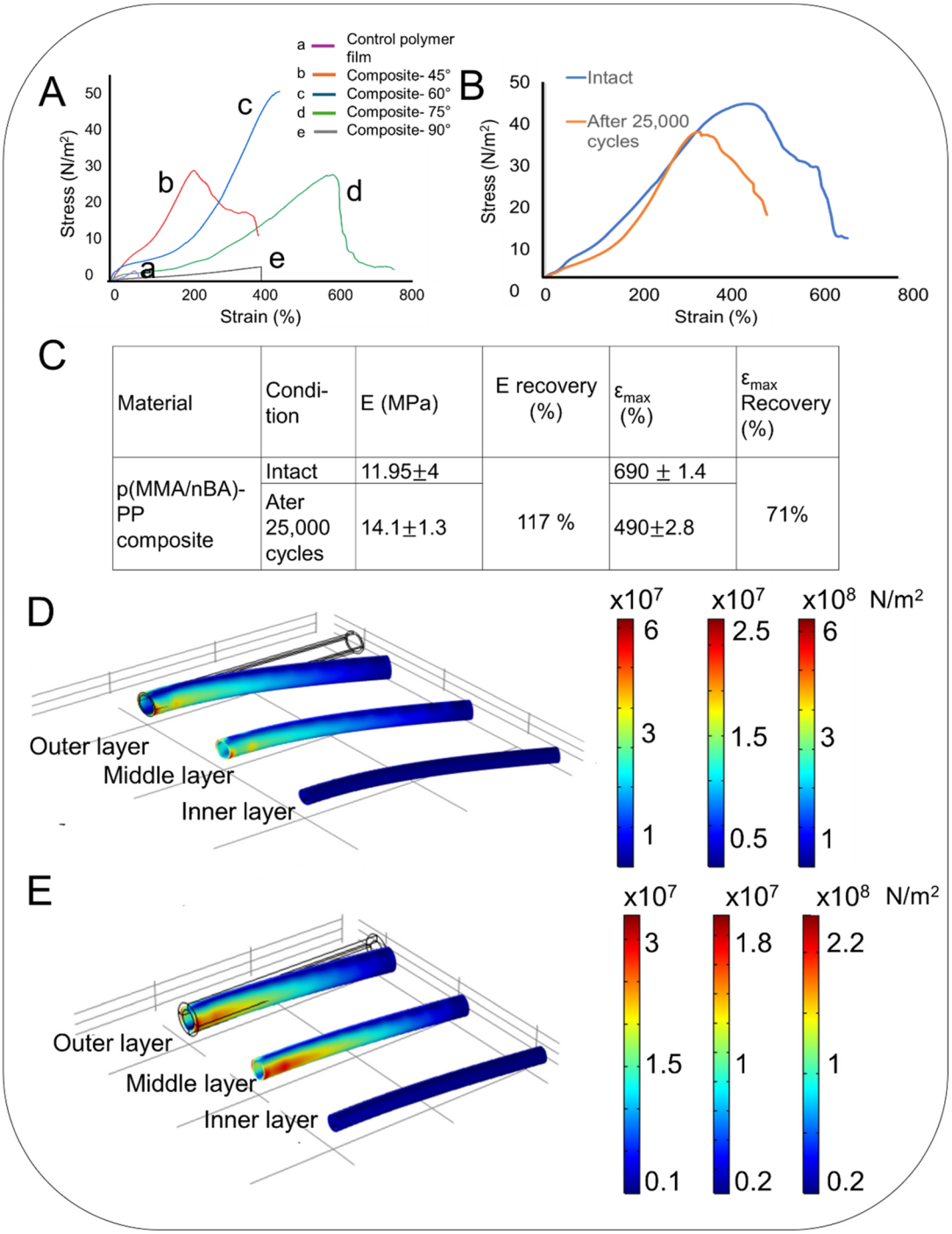

Material	Condition	E (MPa)	E recovery (%)	ε_{max} (%)	ε_{max} Recovery (%)
p(MMA/nBA)-PP composite	Intact	11.95±4	117 %	690 ± 1.4	71%
	Ater 25,000 cycles	14.1±1.3		490±2.8	

Fig. 2 Stress–strain curves obtained using a 100 kN load cell for self-healable 50/50 p(MMA/*n*BA) copolymer films (a), prototype inner layer composite hose with 45 (b), 60 (c), 75 (d) and 90° (e) winding angles (A). Stress–strain curves for intact and repaired prototype inner-layer composite hoses after 25 000 cycles of damage-repair using a robot arm (B). Mechanical properties of intact (curve a) inner layer composite hose and after 25 000 damage-repair cycles (curve b) (C). Von Mises stress distribution in individual layers of the self-healing inner layer composite after applications of a 30 N bending force on the free end (right side) (D). Von Mises stress distribution in individual layers of the non-self-healing inner layer composite after application of a 30 N bending force on the free end (E). Each side color bar represents the stress distribution in the composite hose, with the maximum stress at the top (red) and the lowest at the bottom (blue).

the free end, ultimately leading to catastrophic failure. In contrast, the self-healing matrix inner layers maintain mechanical integrity through ~25 000 bend-release damage-repair cycles.

H_2 fuel is typically stored at approximately −250 °C, but its operational temperatures range from −80 to +100 °C.[47,48] Thus, to assess how temperature affects the self-healing

efficiency, mechanical damage was induced to the inner-layer composite using a 250 mN force. Optical images of the composite hose are shown in Fig. 3: the undamaged composite (Fig. 3A), after exposure to liquid N_2 for 2 hours at −196 °C (Fig. 3B), at ambient temperature (25 °C, Fig. 3C), and at 85 °C (Fig. 3D). After freezing, no healing was observed due to reduced segmental macromolecular mobility, and minor surface cracks appeared as the material became brittle (Fig. 3B). At 25 °C, partial healing with a noticeable reduction in damage depth occurs (Fig. 3C), but at 85 °C self-healing takes place (Fig. 3D). The H_2 fuel inner layer undergoes a severe temperature cycle from −196 °C to 85 °C. Although at lower temperatures segmental mobility prohibits self-repair, elevated temperatures accelerate it. The retention of mechani-

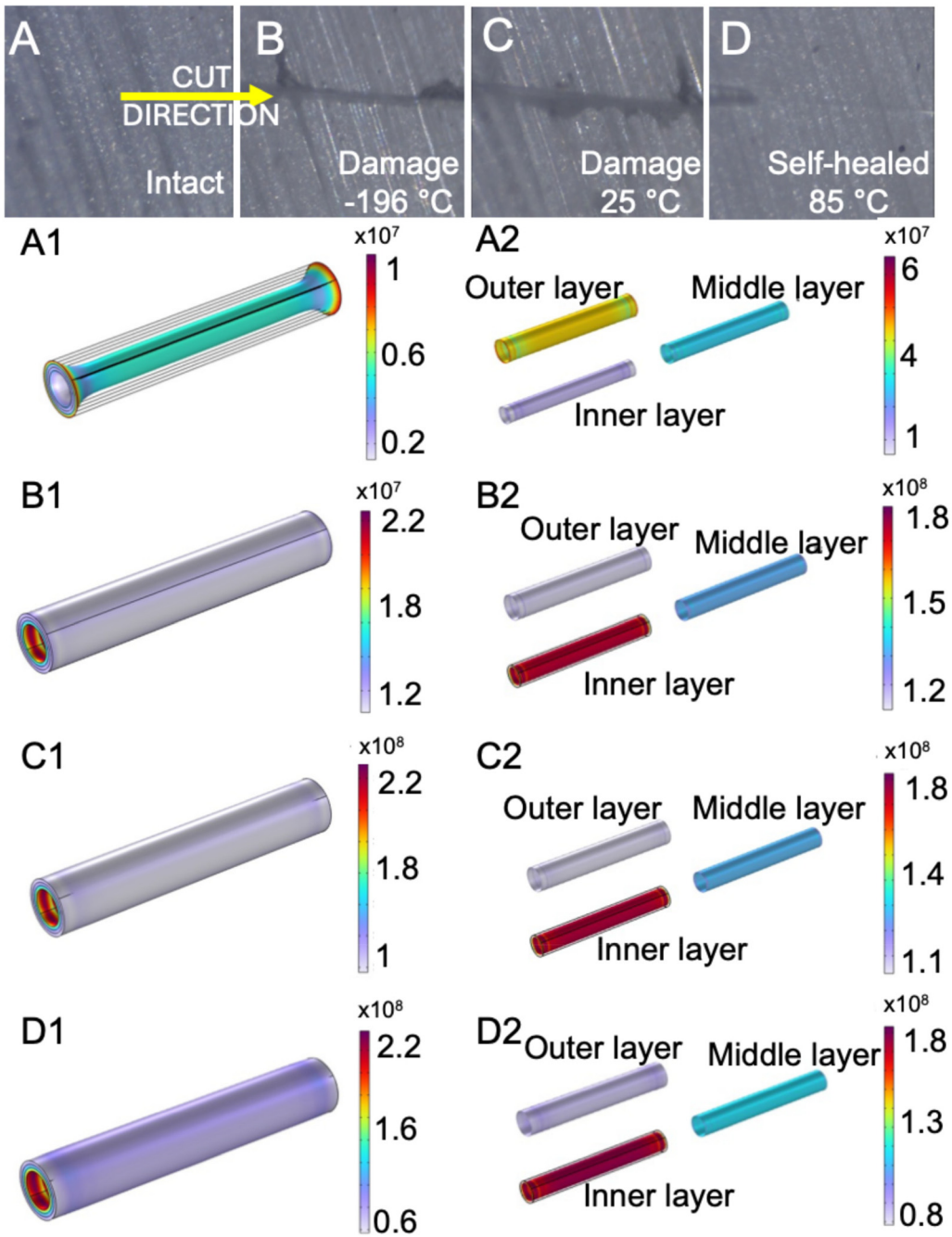

Fig. 3 Intact surface of the prototype inner layer composite (A), mechanically damaged surface of the prototype at −196 °C (liq N_2) (B), damaged surface of the prototype hose at 21 °C ambient (C), and visually self-healed surface of the prototype inner layer composite hose at 85 °C temperatures (D). Distribution of stresses in extracted individual three composite layers carrying H_2 in COMSOL at −40 (A1 and A2), 0 (B1 and B2), 25 (C1 and C2), and 85 °C (D1 and D2) conditions. In these simulations, the bottom left layer represents the innermost layer, the bottom right represents the middle layer, and the outer layer is shown at the top.

cal and chemical integrity is demonstrated in tensile measurements and ^{1}H NMR analysis, as summarized in the SI (Fig. S7, 8 and Table S6).

Parallel molecular dynamics (MD) simulations were performed to identify the effect of H_2 gas on the self-healing of 50/50 MMA/*n*BA copolymers. Since the total cohesive energy density (CED_{total}) is the measure of the energy required to remove a separate macromolecule from its environment, it is anticipated that the presence of H_2 will diminish this energy. Additionally, as the H_2 increases, higher inter-chain separations will lower its values as well as the van der Waals (vdW) contributions to CED_{total} (CED_{vdW}). As shown in SI Fig. S16, the values for CED_{total} and CED_{vdW} decrease upon the addition of H_2 because copolymer chains are separated from each other upon the addition of H_2 molecules, thus lowering the energy of interchain interactions. From the mechanistic standpoint, the drop of the CED values signifies enhanced chain mobility. Upon removal of H_2, the subsequent increase in CED values correlate with recovery inter-chain vdW interactions responsible for reversible self-healing.[37]

Another property of interest for these applications is the heat transfer efficiency of the inner layer. To identify the thermomechanical behavior of these composites under various stress and strain conditions across their cross-sections, a finite-element macroanalysis was conducted.[49] The resulting stress distributions for each composite layer carrying H_2 under deformation at temperatures of −40, 0, 25, and 85 °C are shown in Fig. 3A1, A2, B1, B2, C1, C2, and D1, D2, respectively (Table S7 provides further details). At −40 °C (Fig. 3A1 and A2), overall compression occurs, with the outermost layer exhibiting the highest stress of 4.5×10^7 N m^{-2}, while the innermost layer experiences the lowest stress of 0.11×10^7 N m^{-2}. In contrast, at 0 °C (Fig. 3B1 and B2), the innermost layer carries the highest stress of 18×10^7 N m^{-2}, which gradually decreases to 12×10^7 N m^{-2} toward the outer layer. A similar pattern is observed at 25 °C (Fig. 3C1 and C2), where the stress levels reach a maximum of 18×10^7 N m^{-2} in the innermost layer and drop to 9×10^7 N m^{-2} in the outermost layer. At 85 °C (Fig. 3D1 and D2), the innermost layer continues to carry the maximum stress of 18×10^7 N m^{-2}, while stress in the outermost layer decreases significantly to 0.9×10^7 N m^{-2}. The ring-like stress patterns observed at the inner edges are attributed to the winding, particularly when transitioning from +45° to −45° angles by 90°. Previous studies have shown that poor heat transfer correlates with higher von Mises stress in inorganic crystals. For materials with low thermal conductivity, such as p(MMA/*n*BA), heat is not distributed evenly. Thus, the layer in contact with the heat expands, whereas other layers remain cold. This difference in expansion causes higher stresses at the interface of two layers, leading to poor heat transfer efficiency. These data show that at −40 °C the innermost layer exhibits better heat transfer. In contrast, at elevated temperatures, the outermost layer becomes more efficient, as indicated by the higher stress values, suggesting that layers of this composite exhibit efficient heat transfer under variable thermal conditions in the presence of H_2.

In summary, these studies demonstrate the fabrication of self-healable inner-layer fiber-reinforced composites using a preferentially alternating/random 50/50 p(MMA/*n*BA) commodity copolymer matrix capable of self-healing recovery after more than 25 000 damage-repair cycles. While this work establishes the preliminary mechanical robustness and self-healing ability, future efforts focused on optimizing mechanical properties will further validate the long-term reliability of these systems. The multilayer composites are promising components of larger engineered systems for H_2 fuel delivery and dispensing, retaining mechanical and chemical integrity at extreme conditions.[50] Favorable stress distributions and heat transfer during multiple deformations make them cost-effective and efficient elements for next-generation materials in energy applications.

Conflicts of interest

There are no conflicts of interest to declare.

Data availability

The data supporting the findings of this study are available within the article and its supplementary information (SI). Supplementary information is available. Supporting Documents contain the following: Materials and Methods, Multiphysics simulations (COMSOL), Figure S1–S16, and Tables S1–S7. See DOI: https://doi.org/10.1039/d6lp00079g.

Acknowledgements

This work was supported by the Department of Energy under award DE-EE0008827 and partially by the J.E. Sirrine Foundation at Clemson University. The authors thank Dr Kevin Simmons (Pacific Northwest National Laboratory) and Dr Nalini Menon (Sandia National Laboratories) for their technical assistance.

References

1 H. Sharma, A. Kumar, S. Rana, N. G. Sahoo, M. Jamil, R. Kumar, S. Sharma, C. Li, A. Kumar and S. M. Eldin, *J. Mater. Res. Technol.*, 2023, **26**, 2975–3002.
2 S.-H. Kim, J.-H. Lee, J.-W. Kim, S.-Y. Lee and S.-J. Park, *Adv. Fiber Mater.*, 2022, **4**, 1414–1433.
3 R. Sahu, S. A. Ponnusami, C. Weimer and D. Harursampath, *Polym. Compos.*, 2024, **45**, 9–42.
4 S. Zhandarov and E. Mäder, *Compos. Sci. Technol.*, 2005, **65**, 149–160.
5 Y. Zhou, L. Li, Z. Han, Q. Li, J. He and Q. Wang, *Chem. Rev.*, 2022, **123**, 558–612.
6 L. T. Drzal, in *Epoxy resins and composites II*, Springer, 2005, pp. 1–32.

7 S. Wang, S. Adanur and B. Z. Jang, *Composites, Part B*, 1997, **28**, 215–231.
8 H.-W. Engels, H.-G. Pirkl, R. Albers, R. W. Albach, J. Krause, A. Hoffmann, H. Casselmann and J. Dormish, *Angew. Chem., Int. Ed.*, 2013, **52**, 9422–9441.
9 S. H. Aziz, M. P. Ansell, S. J. Clarke and S. R. Panteny, *Compos. Sci. Technol.*, 2005, **65**, 525–535.
10 B. Ghosh and M. W. Urban, *Science*, 2009, **323**, 1458–1460.
11 L. U. Devi, S. S. Bhagawan and S. Thomas, *J. Appl. Polym. Sci.*, 1997, **64**, 1739–1748.
12 S. M. Sapuan, H. S. Aulia, R. A. Ilyas, A. Atiqah, T. T. Dele-Afolabi, M. N. Nurazzi, A. B. M. Supian and M. S. N. Atikah, *Polymers*, 2020, **12**, 2211.
13 H. L. N. Mcmanus and G. S. Springer, *J. Compos. Mater.*, 1992, **26**, 206–229.
14 J. T. Mottram and R. Taylor, *Compos. Sci. Technol.*, 1987, **29**, 211–232.
15 B. Ghosh, K. V. Chellappan and M. W. Urban, *J. Mater. Chem.*, 2012, **22**, 16104–16113.
16 J. Ling, M. Z. Rong and M. Q. Zhang, *J. Mater. Chem.*, 2011, **21**, 18373–18380.
17 N. Oya, P. Sukarsaatmadja, K. Ishida and N. Yoshie, *N. Polym. J.*, 2012, **44**, 724–729.
18 W. Chen, X. Tao and Y. Liu, *Compos. Sci. Technol.*, 2006, **66**, 3029–3034.
19 E. C. Botelho, Ł. Figiel, M. C. Rezende and B. Lauke, *Compos. Sci. Technol.*, 2003, **63**, 1843–1855.
20 N. J. Capiati and R. S. Porter, *J. Mater. Sci.*, 1975, **10**, 1671–1677.
21 J. Sandler, P. Werner, M. S. P. Shaffer, V. Demchuk, V. Altstädt and A. H. Windle, *Composites, Part A*, 2002, **33**, 1033–1039.
22 A. Tregub, V. Privalko, H. Kilian and G. Marom, *Appl. Compos. Mater.*, 1994, **1**, 167–176.
23 N. G. Karsli and A. Aytac, *Composites, Part B*, 2013, **51**, 270–275.
24 J. Dang, J. Sun and Z. Liu, *Polym. Compos.*, 2024, **45**, 6788–6803.
25 A. Wang, R. Lin, V. K. Polineni, A. Essner, C. Stark and J. H. Dumbleton, *Tribol. Int.*, 1998, **31**, 661–667.
26 M. Luo, X. Tian, J. Shang, W. Zhu, D. Li and Y. Qin, *Composites, Part A*, 2019, **121**, 130–138.
27 E. Pisanova, S. Zhandarov and V. Dovgyalo, *Polym. Compos.*, 1994, **15**, 147–155.
28 R. J. Wojtecki, M. A. Meador and S. J. Rowan, *Nat. Mater.*, 2011, **10**, 14–27.
29 C. N. Bowman and C. J. Kloxin, *Angew. Chem., Int. Ed.*, 2012, **51**, 4272–4274.
30 V. Zhang, B. Kang, J. V. Accardo and J. A. Kalow, *J. Am. Chem. Soc.*, 2022, **144**, 22358–22377.
31 M. Podgórski, B. D. Fairbanks, B. E. Kirkpatrick, M. McBride, A. Martinez, A. Dobson, N. J. Bongiardina and C. N. Bowman, *Adv. Mater.*, 2020, **32**, 1906876.
32 S. Wang, L. Li, Q. Liu and M. W. Urban, *Macromolecules*, 2022, **55**, 4703–4709.
33 M. Delahaye, J. M. Winne and F. E. Du Prez, *J. Am. Chem. Soc.*, 2019, **141**, 15277–15287.
34 K. Yu, Q. Shi, M. L. Dunn, T. Wang and H. J. Qi, *Adv. Funct. Mater.*, 2016, **26**, 6098–6106.
35 S. Gaikwad and M. W. Urban, *J. Am. Chem. Soc.*, 2023, **145**, 9693–9699.
36 S. Gaikwad and M. W. Urban, *Angew. Chem., Int. Ed.*, 2024, **63**, e202405504.
37 M. W. Urban, D. Davydovich, Y. Yang, T. Demir, Y. Zhang and L. Casabianca, *J. Sci.*, 2018, **362**, 220–225.
38 S. Wang and M. W. Urban, *Adv. Sci.*, 2021, **8**, 2101399.
39 D. Ramachandran, F. Liu and M. W. Urban, *RSC Adv.*, 2012, **2**, 135–143.
40 R. R. Barth, K. L. Simmons and C. W. San Marchi, *Polymers for hydrogen infrastructure and vehicle fuel systems*, Sandia National Lab. (SNL-CA), Livermore, CA (United States), 2013..
41 Y. Luo, Y. Wang, Z. Kang, H. Liu, A. Yu, S. Nie and Z. Yang, *Int. J. Hydrogen Energy*, 2024, **110**, 300–309.
42 N. C. Menon and E. Hecht, *Dispenser Reliability: Materials R&D. A Hydrogen Fueling Infrastructure Research and Station Technology (H2FIRST) Report*, Sandia National Lab. (SNL-CA), Livermore, CA (United States), 2020.
43 J. L. Self, C. S. Sample, A. E. Levi, K. Li, R. Xie, J. R. De Alaniz and C. M. Bates, *J. Am. Chem. Soc.*, 2020, **142**, 7567–7573.
44 Y. Heo and H. A. Sodano, *Adv. Funct. Mater.*, 2014, **24**, 5261–5268.
45 S. T. Peters, *Handbook of composites*, Springer Science & Business Media, 2013.
46 C. Multiphysics, *J. Comsol Multiphys.*, 1998, **9**, 32.
47 United Nations Economic Commission for Europe, *Hydrogen Technology Brief*, 2022 [Online], Available: https://unece.org/sites/default/files/2022-02/Hydrogen%20brief_EN_final.pdf.
48 "Hydrogen Storage", IntechOpen, https://www.intechopen.com/journals/7/articles/424.
49 T. Ichimura and M. Hori, *Earthq. Eng. Struct. Dyn.*, 2006, **35**, 395–417.
50 S. Jana, A. Parthiban and W. Rusli, *Chem. Commun.*, 2025, **61**, 3233–3249.